JGR Atmospheres

RESEARCH ARTICLE
10.1029/2018JD029961

Special Section:
Bridging Weather and Climate: Subseasonal-to-Seasonal (S2S) Prediction

Weakening of the Teleconnection From El Niño–Southern Oscillation to the Arctic Stratosphere Over the Past Few Decades: What Can Be Learned From Subseasonal Forecast Models?

Chaim I. Garfinkel[1], Chen Schwartz[1], Amy H. Butler[2,3], Daniela I. V. Domeisen[4], Seok-Woo Son[5], and Ian P. White[1]

[1]Fredy and Nadine Herrmann Institute of Earth Sciences, Hebrew University, Jerusalem, Israel, [2]Cooperative Institute for Research in Environmental Sciences, University of Colorado Boulder, Boulder, CO, USA, [3]NOAA Chemical Sciences Division, Boulder, CO, USA, [4]Institute for Atmospheric and Climate Science, ETH Zürich, Zürich, Switzerland, [5]School of Earth and Environmental Sciences, Seoul National University, Seoul, South Korea

Abstract While a connection between the El Niño–Southern Oscillation (ENSO) and the Northern Hemisphere wintertime stratospheric polar vortex appears robust in observational studies focusing on the period before 1979 and in many modeling studies, this connection is not evident over the past few decades. In this study, the factors that have led to the disappearance of the ENSO-vortex relationship are assessed by comparing this relationship in observational data and in operational subseasonal forecasting models over the past few decades. For reforecasts initialized in December, the models simulate a significantly weaker vortex during El Niño than La Niña (LN) as occurred before 1979, but no such effect was observed to have occurred. The apparent cause of this is the eastern European and western Siberian height anomalies present during ENSO. The observed LN events were associated with persistent ridging over eastern Europe as compared to El Niño. Although the Subseasonal-to-Seasonal models are initialized with this ridge, the ridge quickly dissipates. As ridging over this region enhances wave flux entering the stratosphere, the net effect is no robust stratospheric response to ENSO in the observations despite a North Pacific teleconnection that would, in isolation, lead to less wave flux for LN. The anomalies in the eastern European sector in response to ENSO likely reflect unforced internal atmospheric variability.

Key Points:
- The strength of the connection between the Arctic stratospheric vortex and ENSO has weakened in the past few decades
- The apparent cause of this was height anomalies over eastern Europe; LN events were associated with persistent ridging as compared to EN
- Anomalies in the eastern European sector can modulate the vortex,but this effect likely was not forced by ENSO, rather is internal variability

Supporting Information:
- Supporting Information S1

Correspondence to:
C. I. Garfinkel,
chaim.garfinkel@mail.huji.ac.il

Citation:
Garfinkel, C. I., Schwartz, C., Butler, A. H., Domeisen, D. I., Son, S.-W., & White, I. P. (2019). Weakening of the teleconnection from El Niño–Southern Oscillation to the Arctic stratosphere over the past few decades: What can be learned from subseasonal forecast models? *Journal of Geophysical Research: Atmospheres*, *124*, 7683–7696. https://doi.org/10.1029/2018JD029961

Received 8 NOV 2018
Accepted 20 MAY 2019
Accepted article online 7 JUN 2019
Published online 29 JUL 2019

Author Contributions
Conceptualization: Chaim I. Garfinkel, Chen Schwartz, Amy H. Butler, Daniela I. V. Domeisen, Seok-Woo Son, Ian P. White

1. Introduction

Interannual variability in the tropics is dominated by the El Niño–Southern Oscillation (ENSO), which manifests as anomalous sea surface temperatures in the Pacific Ocean and accompanying changes in precipitation. It has long been known that ENSO impacts the global atmospheric circulation in both the troposphere (Horel & Wallace, 1981; Halpert & Ropelewski, 1992; Ropelewski & Halpert, 1987; Trenberth et al., 1998) and stratosphere (Domeisen et al., 2019). Specifically, the warm (El Niño hereafter EN) phase of ENSO has been associated with an accelerated Brewer-Dobson circulation and a warmer Arctic stratosphere by several kelvin on average (Camp & Tung, 2007; Free & Seidel, 2009; Garfinkel & Hartmann, 2007). In contrast, the cold phase of ENSO (La Niña hereafter LN) is on average associated with a colder Arctic stratosphere (Garfinkel & Hartmann, 2007; Iza et al., 2016) though this cooling is somewhat less robust (Manzini et al., 2006).

The stratospheric response to EN events is driven by a deepened Aleutian low (e.g., Barnston & Livezey, 1987), which constructively interferes with the climatological stationary planetary wave pattern and leads to strengthened wave flux into the stratosphere (i.e., linear interference; Garfinkel & Hartmann, 2008; Garfinkel et al., 2010; Smith et al., 2010; Smith & Kushner, 2012), as recently reviewed by Domeisen et al. (2019). Other modes of tropospheric variability (e.g., October Eurasian snow) can affect the vortex through a similar pathway but via variability over western Siberia/eastern Europe, where a ridge constructively interferes with the climatological stationary planetary wave pattern and leads to strengthened wave flux into the stratosphere (Bao et al., 2017; Cohen & Jones, 2011; Garfinkel et al., 2010; Kretschmer et al., 2017). Episodes

Methodology: Chaim I. Garfinkel, Chen Schwartz, Amy H. Butler, Daniela I. V. Domeisen, Seok-Woo Son, Ian P. White
Writing - Original Draft: Chaim I. Garfinkel
Formal Analysis: Chaim I. Garfinkel
Investigation: Chaim I. Garfinkel
Writing - review & editing: Chaim I. Garfinkel, Chen Schwartz, Amy H. Butler, Daniela I. V. Domeisen, Seok-Woo Son, Ian P. White

of prolonged upward wave flux can lead to sudden stratospheric warming (SSW) events (Polvani & Waugh, 2004; Sjoberg & Birner, 2012), induce a tendency toward a negative phase of the North Atlantic Oscillation (Bell et al., 2009; Ineson & Scaife, 2009), and increase weather predictability (Sigmond et al., 2013) in the Euro-Atlantic region for more than a month.

Over the past few decades the connection between ENSO and the Arctic stratospheric vortex has weakened, and if one examines only the period since 1979 it is not statistically significant in the lower stratosphere (Domeisen et al., 2019; Hu et al., 2017; Yang et al., 2017). Consistent with this, decadal variability is also present in the Atlantic sector response to ENSO, with a negative correlation between ENSO and the North Atlantic Oscillation from 1958 to 1978 and a weak response afterward (Domeisen et al., 2019; Greatbatch et al., 2004). This leads to differences in the precipitation response over Europe to ENSO (Ayarzagüena et al., 2018). The frequency of extreme transient wave activity flux events from the North Pacific to the North Atlantic also changed after 1978 (Jiménez-Esteve & Domeisen, 2018).

Several possible explanations for this decadal variability may exist:

1. Decadal variability in the Pacific or Atlantic Ocean (Gershunov & Barnett, 1998; Hurwitz et al., 2012; Hu & Guan, 2018; Kren et al., 2016; Omrani et al., 2014; Woo et al., 2015).
2. Modulation of the ENSO teleconnection by the quasi-biennial oscillation (QBO): When westerly QBO occurs during EN, both the tropospheric and stratospheric teleconnections are stronger (Calvo et al., 2009; Garfinkel & Hartmann, 2010), and this alignment occurred preferentially before 1979 (Domeisen et al., 2019; Garfinkel & Hartmann, 2007; Hu et al., 2012).
3. Changes in the North Pacific tropospheric anomalies during ENSO: The North Pacific low extended into northeast Asia during the period before 1979 but was confined to the northeast Pacific since 1979 (Domeisen et al., 2019; Hu et al., 2017). A low confined to the northeast Pacific is less efficient in weakening the vortex than a low that extends further west (Garfinkel et al., 2010). In addition, the North Pacific ridge associated with LN has shifted closer to North America since 1979 (Kumar et al., 2010; Yang et al., 2017) where it leads to an enhanced wave-2 signal (Yang et al., 2017).
4. This apparent decadal variability is unforced and rather occurred by chance. Model simulations run over a limited period can also simulate a relative weakening of the ENSO- vortex effect that is reminiscent of that observed, despite showing a robust connection over a longer period (Weinberger et al., 2019)
5. The tendency of EN to be associated with more SSW and LN with fewer SSW events in the first half of this period only but not the second (Butler & Polvani, 2011; Domeisen et al., 2019). Over the entire period there is little difference in the frequency of SSW events between LN and EN winters (Butler & Polvani, 2011; Garfinkel et al., 2012a), though there is sensitivity to how LN events and SSW events are classified (Polvani et al., 2017; Song & Son, 2018).
6. It is possible that there may never have been a strong connection in the first place and the satellite network since 1979 better constrains reanalysis products. Note, however, that many modeling studies using a wide range of models have concluded EN leads to a weaker vortex as compared to LN (Bell et al., 2009; Domeisen et al., 2015; Garfinkel et al., 2012a; Li & Lau, 2013; Manzini et al., 2006; Polvani et al., 2017; Song & Son, 2018; Taguchi & Hartmann, 2006), and therefore, the modeling evidence for such a connection is strong. Also, a mechanistically similar stratospheric response has been found following anomalous convection on intraseasonal time scales (Garfinkel et al., 2012b, 2014; Kang & Tziperman, 2017; Liu et al., 2014; Schwartz & Garfinkel, 2017).

The Subseasonal-to-Seasonal (S2S) Prediction project (Vitart et al., 2017) has recently made available a large number of hindcasts covering the period over which the ENSO-vortex connection is weak. These simulations are all initialized with the observed atmospheric state (including the QBO, Garfinkel et al., 2018) and sea surface temperatures (including any decadal oceanic variability), and as they are intended to be useful for forecasting operationally, they can be compared directly to observed variability during the duration of their forecast.

This study uses the S2S simulations to assess the factors that led to a weak ENSO-vortex connection over the past few decades. After introducing the data and methods in section 2, we establish in section 3 that the ENSO-vortex relationship has weakened recently. We then show in section 4 that the S2S models fail to capture the observed weak ENSO-vortex connection for reforecasts initialized in December despite being initialized with observed oceanic and atmospheric conditions and identify the apparent proximate cause for

Table 1
S2S Model Experiments Chosen

Model (ensemble members)	Years	Reforecasts analyzed	Vertical levels	Model top
CMA (4)	1999–2014	Six per month	40	0.5 hPa
NCEP (4)	1999–2010	Nine per month	64	0.02 hPa
ECMWF (11)	1996–2013	Four per month	91	0.01 hPa
UKMO (3)	1998–2009	Four per month	85	85 km

this failure. We then discuss the implications for the observed weak ENSO-vortex relationship over the past few decades in section 5.

2. Data and Methods

The association between ENSO and polar stratospheric variability is examined in models that have contributed to the S2S Prediction project (Vitart et al., 2017). As the results of this study are based in large part on analyzing the lagged response well beyond a month, we examine models that archive data beyond 44 days. Five modeling centers provided data that met this criterion at the time we started downloading data—the Australian Bureau of Meteorology (BoM), the European Centre for Medium-Range Weather Forecasts (ECMWF), the China Meteorological Administration (CMA), the U.K. Met Office (UKMO), and the National Center for Environmental Prediction (NCEP). As shown in Garfinkel et al. (2018) the BoM model struggles to represent the QBO even in the first week due to its coarse vertical resolution (only 17 levels in the vertical), and as shown by Garfinkel and Schwartz (2017) the BoM model struggles to simulate SSWs as well. Hence, in this paper we do not show results from the BoM model. Table 1 summarizes the reforecasts analyzed in this study. Note that when we downloaded UKMO data, there were only three ensemble members available and fewer calendar years than are currently available. For the ECMWF model we downloaded only one reforecast each week, and for the NCEP model we only downloaded nine reforecasts each month, for consistency with the data availability for the other models. These various forecast systems differ in the quality of their representation of the stratosphere: The stratosphere is less well resolved in CMA as compared to the other three forecast systems (Table 1).

We consider forecasts initialized in November through February and assess the stratospheric response to ENSO up to 2 months later, though the main focus is on reforecasts initialized in December in order to focus on the period when the zonal wind at 10 hPa and 60°N response to EN is strongest (Figures 6 and 7 of Calvo et al., 2017). Figures for other months are shown in the supporting information. Taking the ECMWF reforecasts in December, for example, we first determine if the first date of each reforecast in December over the period of data availability is during an EN winter or a LN winter. Reforecasts are characterized as EN or LN if the value of the observed Niño3.4 index in monthly mean ERSSTv5 data (Huang et al., 2017) for the calendar month which contains the day of initialization is warmer than 0.5 K (for EN) or colder than −0.5 K (for LN). We only select initializations in which the zonal mean zonal wind at 60°N, 10 hPa (U10) is above 10 m/s in order to avoid selecting vortex states that are already highly disturbed where nonlinear wave effects are most pronounced, and results are similar if we use, for example, 5 or 12 m/s. We then form composites of all reforecasts initialized during EN conditions and during LN conditions and examine the extratropical response for the duration of the reforecast. We then form corresponding EN and LN composites based on these same dates but using atmospheric data from the MERRA (Modern-Era Retrospective Analysis for Research and Applications; Rienecker et al., 2011) reanalysis and compare the extratropical response in the reforecasts to the observed extratropical response in order to assess the fidelity of ENSO teleconnections in the ECMWF forecast system. We thereby subsample MERRA data to match the ECMWF forecast system.

A similar procedure is followed for the other forecast systems. Note that each modeling center has made available reforecasts from different years and the restart dates differ among the modeling centers even for a given year. It is therefore necessary to separately composite the observations according to the actual initializations used for each model in order to more meaningfully compare the modeled and observed stratospheric response to ENSO.

We examine the following metrics of the extratropical circulation in order to assess the strength of the ENSO-vortex connection: zonal wind at 10 hPa and 60°N (U10); 70°N and poleward area-weighted aver-

aged temperature at 50 hPa (T50); 70°N and poleward area-weighted averaged geopotential height at 100 hPa (Z100); heat flux ($\overline{v'T'}$) at 500a and 100 hPa area-weighted from 40°N to 80°N for zonal wavenumbers 1 and 2. U10 is conventionally used to define SSW events (Butler & Gerber, 2018; Charlton & Polvani, 2007), and together with polar cap geopotential height is tightly coupled to the Northern Annular Mode (Baldwin & Thompson, 2009). The heat flux is proportional to the vertical component of the Eliassen-Palm flux, and hence, heat flux at 100 hPa is a proxy for wave activity in the lower stratosphere and subsequent stratospheric variability (e.g., Newman et al., 2001). Anomalous heat flux at 100 hPa can alternately reflect altered conditions for wave propagation within the stratosphere or altered wave generation in the troposphere (Cámara et al., 2017; White et al., 2019), and hence, we also examine 500-hPa heat flux to better connect ENSO to its stratospheric response. The 100-hPa heat flux peaks between 40°N and 80°N, and hence, we focus on this latitude band (Garfinkel et al., 2012a). Note that the S2S database only contains data at three stratospheric levels (10, 50, and 100 hPa), which necessarily limits our ability to diagnose the mechanism behind the connection of ENSO with the vortex. We show the weekly average for each of the aforementioned indices in our figures.

Statistical significance of the difference between EN and LN is determined using a two-tailed difference of means Student's t test, and the null hypothesis throughout is that there is no difference between EN and LN. For the S2S models each reforecast ensemble member is treated as a separate degree of freedom as we are interested in the extratropical response after the first week when internal variability already leads to differences among the ensemble members. For MERRA, each winter is treated as a separate degree of freedom to avoid double-counting the same observed data for different initialization dates.

The statistical significance of running correlations between ENSO and variables of interest (e.g., U10) is computed via a Monte Carlo technique. We first use Burg's method to fit an AR-2 process to the Nino3.4 index from 1958 to 2017; we use Burg's method following De Hoon et al. (1996), and the relevance of an AR-2 process for ENSO has been demonstrated by Vimont et al. (2002). We then generate 3,000 realizations of an AR2 process with the same statistical properties as ENSO and compute the running correlation of each of these random processes with U10 for all possible 25-year periods between 1958 and 2017. We evaluate the difference in the correlation (Δ correlation) between each 25-year period and the most recent 25 years for each realization. We then compute the top and bottom 2.5% quantiles of the maximum and minimum Δ correlation without making any assumption on the nature of the distribution and hence form 95% confidence intervals of the Δ correlation of ENSO with subpolar stratospheric winds.

Rank histograms (Hamill, 2001) are used to compare the ECMWF response to the observed response of U10. For every initialization in the reforecast period, we sort the ensemble members by their response in the sixth week and evaluate where MERRA would rank if we treat it as an "extra" ensemble member. If it falls between, for example, ensemble members 4 and 5, then we increment the bar that falls between 4 and 5 by 1. We compute the rank histogram for initializations during EN and LN separately. We assess the likelihood of a rank histogram occurring by chance with the following Monte Carlo test. Suppose, for example, there are 66 initializations of a given ENSO phase. We then select 66 random numbers evenly distributed between 1 and 12, form a histogram of the response, and then compute the difference in population of the two leftmost and two rightmost bins. Results are identical if we select the three or four leftmost and rightmost bins. This procedure is repeated 3,000 times, and by computing the top and bottom 2.5% quantiles of the maximum and minimum difference, we form 95% confidence intervals of the deviation of the population of the leftmost bins from the rightmost bins in a rank histogram.

The statistical significance of differences in variables of interest (e.g., U10) to EN versus LN in the S2S forecast systems as compared to MERRA is also computed via a Monte Carlo resampling technique. For each S2S forecast systems,

1. Step 1: We randomly select initializations from the full hindcast ensemble to match the number of actual EN and LN initializations, without allowing the same initialization to be placed in both the EN and LN fictitious samples.
2. Step 2: We then compute the difference in U10 for these fictitious EN and LN samples both for the model and for MERRA reanalysis.
3. Step 3: We then compute the difference in U10 between the model and MERRA responses for these fictitious composites.

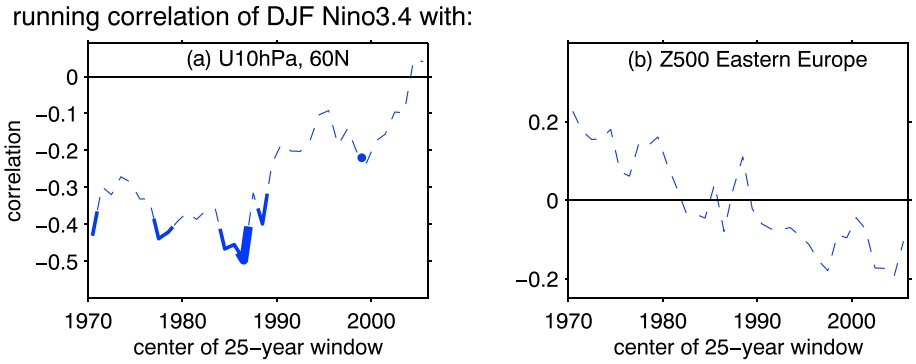

Figure 1. Running correlations over 25-year windows between Niño3.4 in DJF and extratropical variability sourced from the JRA-55 reanalysis in (a) zonally averaged zonal wind at 60°N in DJF at 10 hPa from the JRA-55 reanalysis; (b) Z500 in the eastern European region defined here as 35–45°E,55–65°N, following Garfinkel et al. (2010). Thick (thin) lines indicate statistical significance at the 95% (90% level) for a 25-year correlation as given by the Monte Carlo test described in section 2. Significance is shown only for periods in which no more than half of the samples being compared overlap. Panel (a) is after Figure 13c in Domeisen et al. (2019). DJF = December–February.

4. Step 4: Steps 1 through 3 are repeated 3,000 times, with different initializations randomly included in the fictitious EN and LN composites. We then compute the top and bottom 2.5% quantiles of the maximum and minimum difference between the S2S forecast systems and MERRA without making any assumption on the nature of the distribution, to which we compare the actual difference between the S2S forecast systems and observations.

3. Recent Weakening of the Observed Connection Between ENSO and the Arctic Stratosphere

We begin by revisiting the key result of Hu et al. (2017) and Yang et al. (2017): Over the past few decades, the relationship between ENSO and the Arctic stratospheric vortex has weakened. Figure 1a shows running correlations over 25-year windows between Niño3.4 in December–February and U10, and Figure 1a indicates that while EN was associated with weaker subpolar stratospheric westerly winds as compared to LN before 1990, this effect has since weakened and has even reversed over the most recent 25 years. The correlation is essentially zero if we focus on the period 1999 to 2009, the period common to the S2S models ($r = 0.03$ for U10), when several SSW events occurred during LN. The statistical significance of this weakening is assessed with the Monte Carlo test described in section 2. In Figure 1a, solid lines are used for 10% and thick lines are used for 5% significance. The correlation between ENSO and the Arctic stratospheric vortex was significantly different at the 5% significance level for 25-year periods centered in the 1980s as compared to the most recent period. Similar nonstationarity is evident with slight changes in the variables compared (see Figure 13c in Domeisen et al., 2019) or the length of the averaging window.

The field significance of the running correlation can be assessed by first converting the correlation for each central date into a Z score using a Fisher-z transformation, computing the difference of the Z score between each central date and the most recent 25 years to compute a ΔZ, summing the ΔZ scores across all central dates to form a cumulative ΔZ score, and then comparing the cumulative ΔZ score for each of the 3,000 Monte Carlo realizations to the observed cumulative ΔZ score. The observed cumulative ΔZ score is more extreme than in all but 4.3% of the 3,000 Monte Carlo realizations.

This paper tries to answer the question of why the ENSO-vortex relationship has weakened over this period (and is essentially nonexistent over 1999 to 2009) by considering models that are initialized during ENSO conditions with the observed atmospheric state.

4. Can the S2S Models Capture the Observed Weakening of the ENSO-Vortex Relationship?

We assess whether the ECMWF model, the model with the most ensemble members, simulates a response to ENSO that is consistent with the observed response to ENSO with a rank histogram in Figure 2a for EN and Figure 2b for LN (see section 2). If the bars are concentrated on the right side of a panel, then the observed

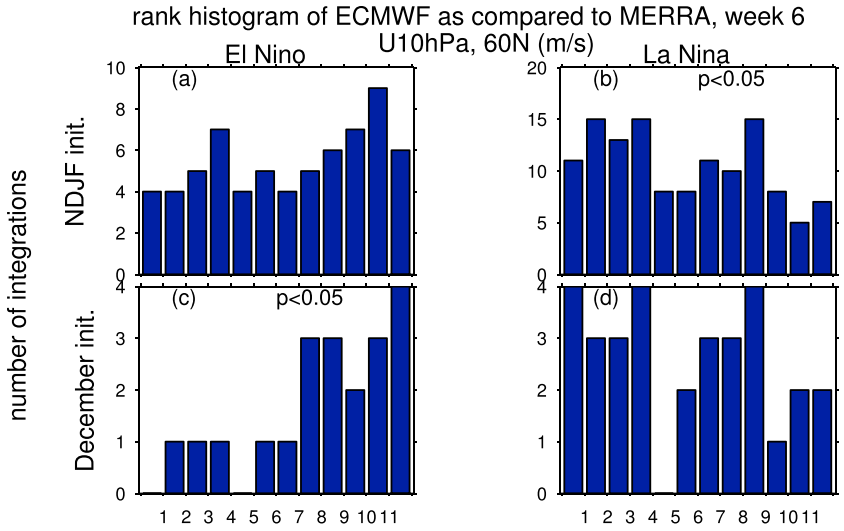

Figure 2. Rank histogram of ECMWF reforecasts as compared to MERRA reanalysis for start dates in (a, b) NDJF and (c, d) December for zonal mean zonal wind at 60°N, 10 hPa in the sixth week after initialization. The left column is for reforecasts initialized during El Niño, and the right column is for reforecasts initialized during La Niña. NDJF = November through February; ECMWF = European Centre for Medium-Range Weather Forecasts; MERRA = Modern-Era Retrospective Analysis for Research and Applications.

U10 for that particular ENSO phase is systematically more westerly than that simulated by the model, and vice versa if the bars are concentrated on the left side of a panel. There is a tendency for MERRA to have faster U10 than most ensemble members for EN, reflected by the fact that most of the bars are to the right of the panel in Figure 2a. In contrast, for LN, MERRA tends to have weaker U10 than most ensemble members, reflected by the fact that most of the bars are to the left of the panel in Figure 2b. These systematic tendencies for overly weak U10 during EN and overly strong U10 during LN in ECMWF are evident when considering all initializations from November to February but are strongest in December (compare the top and bottom rows). For both Figures 2b and 2c we can negate a null hypothesis that the rank histogram is flat at $p < 0.05$ using the Monte Carlo test for rank histograms described in section 2.

Figure 3 generalizes the results of Figure 2 for a range of forecast leads and for multiple variables of interest for the ECMWF model, the model with the most ensemble members. We first compute the mean U10 in the ECMWF model (black) for all EN reforecasts initialized in December for each ensemble member (e.g., average of member 1, average of member 2) and thereby average over interannual variability. We then sort the mean response to EN for each of the 11 ensemble members and indicate in Figure 3a the response in the ensemble members with the maximum and minimum response with black dots, and the range encompassed by the seven ensemble members with the response closest to the ensemble mean is indicated with a vertical black line. The observed response for the specific dates included in the model composite is indicated in orange. For U10, the envelope of the model response does not encompass the observed response for EN by the second week after initialization. For Z100 (Figures 3c, and 3d), the envelope of the model response does not encompass the observed response for LN by the second week after initialization. Therefore, in December, the ECMWF model fails to capture the observed response to ENSO. In the rest of this paper we explore why the model shows an overly strong vortex in LN as compared to EN, and we then consider whether this can illuminate the causes of the observed weak ENSO-vortex relationship over this period. As the specific ENSO phase most responsible for this failure is sensitive to the stratospheric metric examined, we hereafter focus on the difference between EN and LN.

Figure 4 summarizes the relationship between ENSO and the vortex for the ensemble mean of all models for December initialization dates. The left column of Figure 4 shows the LN-EN difference for each model as a function of forecast week, and dots indicate that the modeled responses to EN and LN are significantly different. The right column of Figure 4 shows the difference in MERRA subsampled to match the specific dates included in each composite for each model, and dots indicate that there is a significant differ-

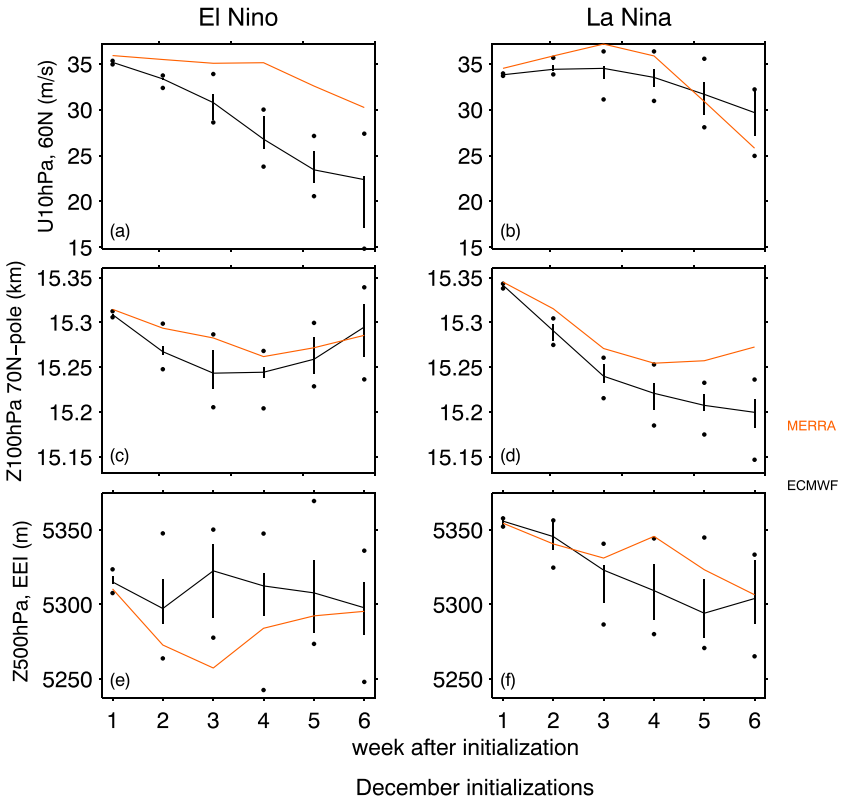

Figure 3. Fidelity of the response to El Niño–Southern Oscillation in the ECMWF reforecasts as compared to MERRA reanalysis for start dates in December for (a, b) zonal mean zonal wind at 60°N, 10 hPa; (c, d) area-weighted average of geopotential height at 100 hPa from 70°N to the pole; (e, f) 500-hPa geopotential height over eastern Europe, defined here as 35–45°E,55–65°N, following Garfinkel et al. (2010). The left column is for El Niño, and the right column for La Niña. The response in the ensemble members with the maximum and minimum response is indicated with black dots, and the range encompassed by the seven ensemble members with the response closest to the ensemble mean is indicated with a vertical black line.

ence between the modeled and observed response to ENSO as given by the Monte Carlo test described in section 2.

We begin by assessing whether the models show an effect of ENSO on U10. For the three models with decent stratospheric resolution (UKMO in red, ECMWF in black, and NCEP in green), there is a wide divergence between the model and reanalysis in the U10 response to ENSO around a month after December initializations, with the models indicating a significantly stronger vortex in LN as compared to EN, though no such effect was observed. This difference between the models and observations is statistically significant as given by the Monte Carlo test described in section 2. The CMA model (cyan) fails to show any stratospheric response to EN as compared to LN, but CMA also fails to capture the observed response for CMA initialization dates (cf. cyan curve in left and right columns). Results are similar for T50 and Z100 (Figures 4c–4f): The UKMO, ECMWF, and NCEP models indicate that LN leads to lower heights and colder temperatures over the pole than EN around a month after December initializations, but no such effect was observed.

In contrast, in November, the S2S models more closely simulate the observed response (Figure S1 in the supporting information), though there are discrepancies in January and February (Figures S2 and S3). For example, the U10 response in January is small in S2S models but quite negative in MERRA for most models, and for the Z100 response in February, the S2S models have the wrong sign after week 2. However, the discrepancies between the models and observations are most pronounced in December, and we focus on December for the rest of this study.

This discrepancy between models and observations is also evident in the frequency of easterlies at 10 hPa, 60°N. Figure 5 shows the fraction of reforecasts which simulate easterly U10 at least 1 day out of the forecast week for reforecasts initialized in December. The left column is for the S2S models, and the right column

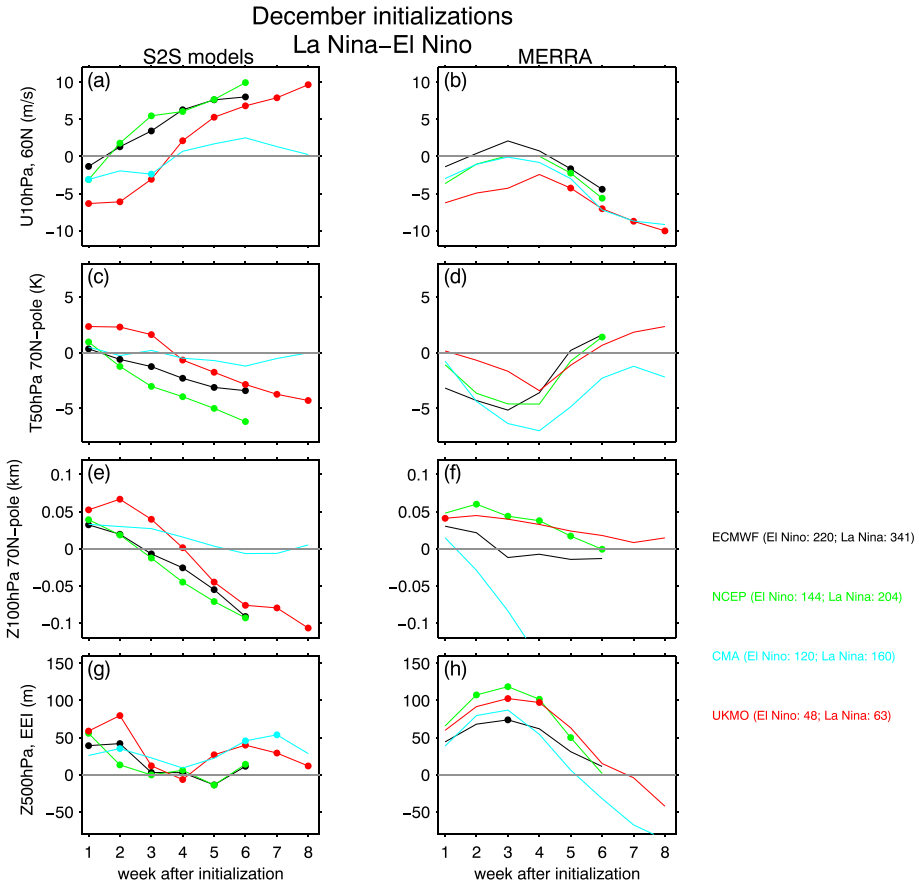

Figure 4. Difference between La Niña and El Niño (La Niña-El Niño) for four different S2S models as a function of forecast week for reforecasts initialized in December. Difference of means between La Niña and El Niño that are statistically significant at the 95% confidence level as given by a Student's *t* test are denoted with dots on the left column; for the right column dots indicate that there is a significant difference between the modeled and observed response to ENSO as given by the Monte Carlo test described in section 2. (a, b) Zonal mean zonal wind at 60°N, 10 hPa; (c, d) area-weighted average of temperature at 50 hPa; (e, f) area-weighted average of geopotential height at 100 hPa from 70°N to the pole; and (g, h) 500-hPa geopotential height over eastern Europe, defined here as 35–45°E, 55–65°N, following Garfinkel et al. (2010). The left column is for the S2S models, and the right column is for MERRA subsampled to match the specific dates included in each composite for each model. The number of reforecast ensemble members for each model and ENSO phase is indicated on the figure legend. MERRA = Modern-Era Retrospective Analysis for Research and Applications; ECMWF = European Centre for Medium-Range Weather Forecasts; NCEP = National Center for Environmental Prediction; CMA = China Meteorological Administration; ENSO = El Niño–Southern Oscillation; S2S = Subseasonal-to-Seasonal.

is for the corresponding days in the MERRA reanalysis. The UKMO, ECMWF, and NCEP models simulate more frequent subpolar easterlies during EN (top row) than during LN (bottom row), while in reanalysis data easterlies were more frequent during LN. This effect is somewhat weaker if one focuses on the frequency of easterlies at 10 hPa, 65°N (Figure S4; consistent with Song & Son, 2018) and is also weaker in other wintertime calendar months (not shown).

The model-observations mismatch in December can be traced back to the heat flux response to ENSO at 500 and 100 hPa (Figure 6), a proxy for upward propagating wave flux. In the three models with decent resolution (UKMO, ECMWF, and NCEP), EN leads to more wavenumber 1 and 2 heat flux than LN at both 500 and 100 hPa. However, in reanalysis data LN (if anything) is associated with more planetary wave flux at 500 hPa. At 100 hPa, higher heat flux was present in observations during LN for later lags, while the models simulate the opposite.

What explains the divergence in response in tropospheric planetary wave driving between the models and observations evident in Figure 6? We answer this by focusing on the tropospheric teleconnections of ENSO in Figure 7. The left column shows the 500-hPa height anomalies associated with ENSO in the NCEP refore-

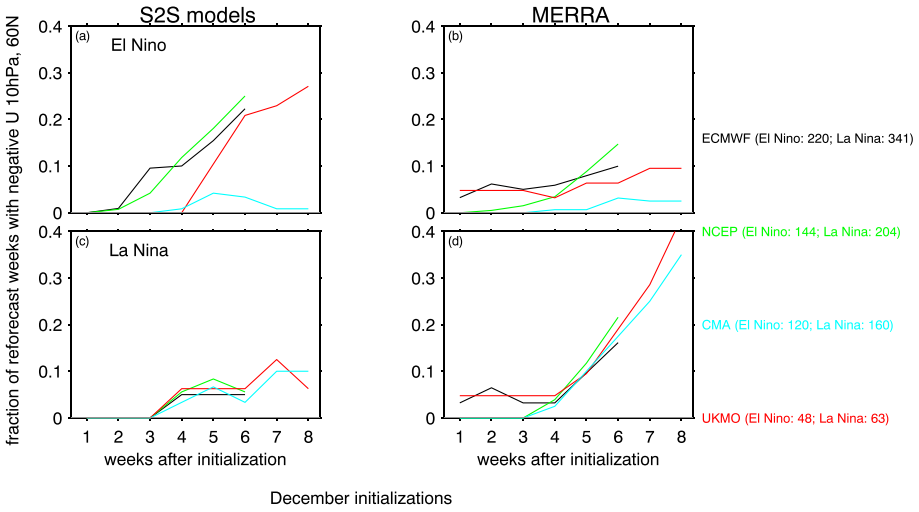

Figure 5. Fraction of reforecasts that contain at least one day per week in which the zonal wind at 10 hPa, 60°N is easterly for four different S2S models for reforecasts initialized in December. The left column is for the S2S models, and the right column is for MERRA subsampled to match the specific dates included in each composite for each model. The number of reforecast ensemble members for each model and El Niño–Southern Oscillation phase is indicated on the figure legend. S2S = Subseasonal-to-Seasonal; MERRA = Modern-Era Retrospective Analysis for Research and Applications; ECMWF = European Centre for Medium-Range Weather Forecasts; NCEP = National Center for Environmental Prediction; CMA = China Meteorological Administration; UKMO = U.K. Met Office.

casts, and the right column shows the corresponding observed response. We focus here on NCEP reforecasts as the ensemble mean of the NCEP reforecasts appears to capture the North Pacific response to ENSO better than the ensemble mean of the ECMWF reforecasts (shown in Figure S5). In the North Pacific the NCEP model simulates a quantitatively similar response to that observed, and hence, the model-observations discrepancy in heat flux is apparently not due to differences in the North Pacific teleconnections of ENSO. In contrast, there are large differences in the European sector response in December, with ridging evident in reanalysis data over eastern Europe in the LN-EN difference for nearly a month; while this feature appears in week 1 in the models, it quickly decays. Similar results are evident for the UKMO and ECMWF models (Figures S5 and S6). Figures 4g and 4h summarize the response over eastern Europe (defined here as 35–45°E, 55–65°N, following Garfinkel et al., 2010) in the S2S models and in reanalysis data, the region

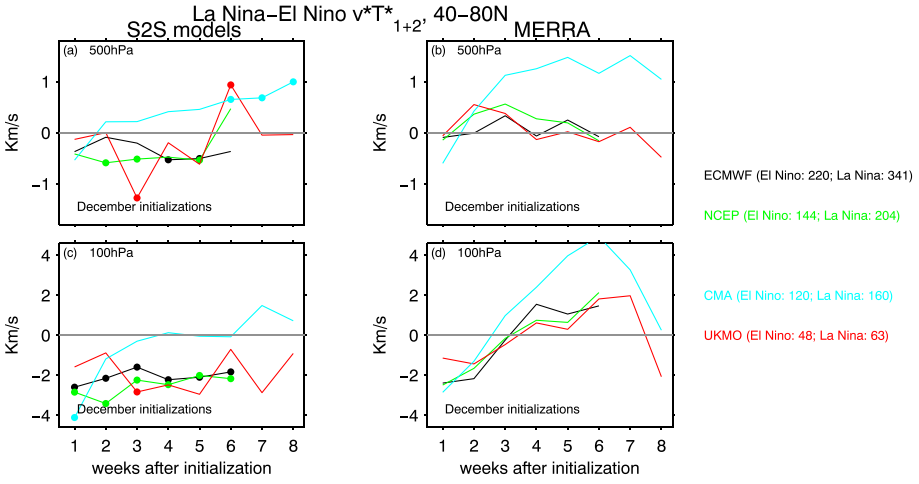

Figure 6. Area-weighted average of wavenumber 1 and 2 heat flux ($\overline{v'T'}$) at 500 and 100 hPa from 40°N to 80°N for initialization dates in December for the S2S models and MERRA.Statistical significance is indicated as in Figure 4. S2S = Subseasonal-to-Seasonal; MERRA = Modern-Era Retrospective Analysis for Research and Applications; ECMWF = European Centre for Medium-Range Weather Forecasts; NCEP = National Center for Environmental Prediction; CMA = China Meteorological Administration; UKMO = U.K. Met Office.

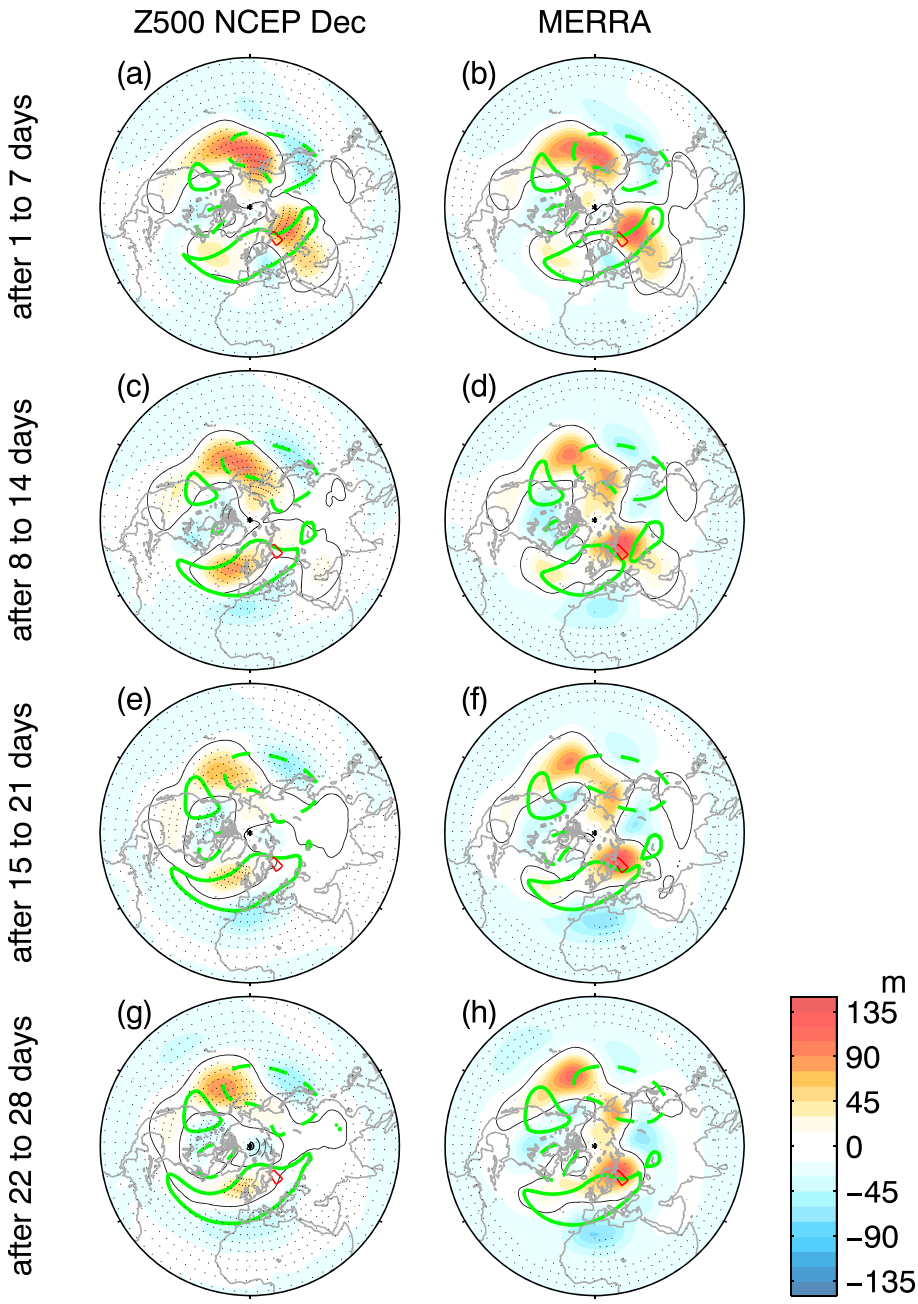

Figure 7. Anomalies (La Niña-El Niño) in Z500 for initializations in December in the NCEP model in the (a, b) first week, (c, d) second week, (e, f) third week, and (g, h) fourth week after initialization. The right is for MERRA subsampled to match the dates chosen for NCEP. Difference of means between La Niña and El Niño that are statistically significant at the 95% confidence level as given by a Student's *t* test are denoted with dots. The zero line is indicated in black. The 70-m contour of the climatological eddy height field is indicated in green. The region 35–45°E,55–65°N is indicated with a red box. S2S = Subseasonal-to-Seasonal; MERRA = Modern-Era Retrospective Analysis for Research and Applications; ECMWF = European Centre for Medium-Range Weather Forecasts; NCEP = National Center for Environmental Prediction; CMA = China Meteorological Administration; UKMO = U.K. Met Office.

shown with a red box in Figure 7; while in the first week a ridge is present due to the initialization of these models, the ridge quickly dissipates in all S2S models, and the difference between the models and observations is statistically significance in week 3. The climatological stationary planetary waves are shown in green in Figure 7 and include a strong ridge over western Siberia and eastern Europe. An anomalously strong eastern European ridge constructively interferes with the climatological planetary waves and contributes to enhanced wave driving of the vortex, and hence, in the reanalysis data LN leads to just as much (if not more) heat flux as EN despite the North Pacific ridge over the past few decades.

Note that this difference in the strength of the ridge between EN and LN is due to model failure in both EN and LN (Figures 3e and 3f), as in both phases the model response differs from that observed. While ENSO and the variability over eastern Europe are negatively correlated over the most recent several decades, in the 1960s and 1970s the correlation was positive (i.e., a ridge preferentially during EN; Figure 1b), and hence, this change in the eastern European sector response to ENSO is consistent with an observed weakening of the ENSO teleconnection to the Arctic stratosphere. As the S2S models fail to simulate this eastern European sector response to ENSO, they also fail to simulate a weakening of the ENSO teleconnection to the Arctic stratosphere.

5. Discussion and Summary

Polar stratospheric variability has important implications for surface climate (Baldwin & Dunkerton, 1999; Limpasuvan et al., 2004; Polvani & Kushner, 2002), and hence, it is crucial to understand the time scale over which polar stratospheric variability can be predicted. ENSO specifically modulates surface climate in parts of the extratropics via its polar stratospheric teleconnection (Butler et al., 2014; Polvani et al., 2017), and therefore, the ENSO-vortex connection can provide skill for seasonal forecasting (Butler et al., 2016; Domeisen et al., 2015).

Over the past few decades, there is little observed difference in vortex strength between EN and LN. Consistent with this, planetary wavenumber heat flux in both the troposphere and stratosphere is similar for EN and LN in observations over this time period (Figure 6). Here we argue that this similarity in vortex wave driving is due to the tropospheric anomalies present in the European sector in December that mitigated the well-known influence of ENSO on the polar stratosphere via the North Pacific (e.g., Garfinkel & Hartmann, 2008; Ineson & Scaife, 2009), such that the vortex wave driving was little different between EN and LN. In contrast, the S2S models show enhanced heat flux in both the troposphere and stratosphere for EN as compared to LN. This model-observations discrepancy in heat flux does not appear to be due to the North Pacific teleconnection of ENSO but is rather consistent with differences in the eastern European sector (Figure 7).

Is the apparent response to ENSO in the European sector unforced or forced by ENSO? We have examined wave activity fluxes following Takaya and Nakamura (2001) for EN and LN in both reanalysis data and S2S models, and there does not appear to be any wave train that originates in the tropical Pacific and ends in the eastern European sector (cf. Jiménez-Esteve & Domeisen, 2018). Consistent with this, the general circulation model simulations of Shaman and Tziperman (2016) with an idealized ENSO forcing find little evidence of a wave train into this region. Furthermore, this ridge does not appear in composites of the observational response to ENSO in longer data sets that include the period before the S2S database begins (Shaman, 2014); the correlation between ENSO and Z500 over eastern Europe is essentially zero if the full JRA-55 reanalysis record is examined (Figure 1b) and is not statistically significant over the most recent several decades. This ridge also does not appear in other wintertime calendar months in the S2S period (not shown), and the lack of this feature in other months is consistent with the stronger correspondence between the modeled response to ENSO and the observed response to ENSO in these other months. That being said, the S2S models are initialized with ridging over eastern Europe in the composited difference LN-EN but fail to maintain it as in observations. We cannot rule out the possibility that model deficiencies in, for example, the representation of blocking in this region (biases are present in CMIP5 models and persist even at high resolutions; Dunn-Sigouin & Son, 2013; Masato et al., 2013; Schiemann et al., 2017) may have led to the modeled rapid decay in height anomalies in this region; this possibility deserves future research, though a thorough investigation of blocking frequency and duration in S2S models, or of the effect of climate change on blocking in this region, is beyond the scope of this work. However, connections between ENSO and blocking in western Eurasia are weak (Cheung et al., 2012; Gollan & Greatbatch, 2017), and hence, even the ridging over western

Siberia/eastern Europe apparent in the composited difference LN-EN appears to reflect internal midlatitude atmospheric variability and not a forced response to ENSO.

The S2S models capture a strong ENSO-vortex connection despite being initialized with observed SSTs and the observed QBO and despite simulating a realistic response to ENSO in the North Pacific sector. Hence, while it is possible that the weakening of the ENSO-vortex connection over the past few decades in months other than December is due to changes in characteristics of ENSO events, oceanic decadal variability, aliasing with the QBO, or an eastward shift in the North Pacific response to ENSO, these four possibilities are certainly not sufficient to explain the recent weak relationship at least in December. Rather, variability in the European sector appears to be a key ingredient.

The weakening of the ENSO-vortex connection over the past few decades is also reflected in SSW frequency during each ENSO phase, with SSW preferentially occurring during LN recently (Butler & Polvani, 2011; Domeisen et al., 2019). In contrast, the S2S models simulated more frequent polar stratospheric easterlies during EN over this period (Figure 5). This discrepancy between the models and observations as to which ENSO phase preferentially leads to more SSW is consistent with the discrepancy in the ridging over eastern Europe (Bao et al., 2017; Cohen & Jones, 2011; Garfinkel et al., 2010; Kretschmer et al., 2017).

Overall, these results highlight that careful attention must be paid to the years included in an observational composite, as studies focusing on different periods could reach opposing conclusions. The observed weakness of the ENSO-vortex connection in the period of 1996 through 2013 is, at least in part, associated with the tropospheric anomalies present during ENSO in the European sector. As these tropospheric anomalies are well removed from the main ENSO teleconnections and are not forced directly by ENSO, it is reasonable to suppose that the weakening of the ENSO-vortex teleconnection over the past few decades (at least in early winter) reflects sampling variability.

Acknowledgments

C. I. G., C. S., and I. P. W. are supported by the Israel Science Foundation (Grant 1558/14) and by a European Research Council starting Grant under the European Unions Horizon 2020 research and innovation program (Grant agreement 677756). D. D. is supported by the Swiss National Science Foundation through Grant PP00P2_170523. S.-W. Son's work is partly supported by the Basic Science Research Program through the National Research Foundation (NRF) funded by the Ministry of Science and ICT (2017R1E1A1A01074889). We thank the three anonymous reviewers for their helpful comments. Correspondence is to be addressed to C. I. G. This work is based on S2S data. S2S is a joint initiative of the World Weather Research Programme (WWRP) and the World Climate Research Programme (WCRP). The original S2S database is hosted at ECMWF as an extension of the TIGGE database, and can be downloaded from the ECMWF server (http://apps.ecmwf.int/datasets/data/s2s/levtype=sfc/type=cf/).

References

Ayarzagüena, B., López-Parages, J., Iza, M., Calvo, N., & Rodríguez-Fonseca, B. (2018). *Stratospheric role in interdecadal changes of El Niño impacts over Europe*, vol. 52, pp. 1173–1186. https://doi.org/10.1007/s00382-018-4186-3

Baldwin, M. P., & Dunkerton, T. J. (1999). Propagation of the Arctic Oscillation from the stratosphere to the troposphere. *Journal of Geophysical Research*, *104*(D24), 30,937–30,946.

Baldwin, M. P., & Thompson, D. W. J. (2009). A critical comparison of stratosphere-troposphere coupling indices. *Quarterly Journal of the Royal Meteorological Society*, *135*, 1661–1672.

Bao, M., Tan, X., Hartmann, D. L., & Ceppi, P. (2017). Classifying the tropospheric precursor patterns of sudden stratospheric warmings. *Geophysical Research Letters*, *44*, 8011–8016. https://doi.org/10.1002/2017GL074611

Barnston, A. G., & Livezey, R. E. (1987). Classification, seasonality and persistence of low-frequency atmospheric circulation patterns. *Monthly Weather Review*, *115*, 1083–1126.

Bell, C. J., Gray, L. J., Charlton-Perez, A. J., Joshi, M. M., & Scaife, A. A. (2009). Stratospheric communication of El Niño teleconnections to European winter. *Journal of Climate*, *22*, 4083–4096. https://doi.org/10.1175/2009JCLI2717.1

Butler, A. H., Arribas, A., Athanassiadou, M., Baehr, J., Calvo, N., Charlton-Perez, A., et al. (2016). The climate-system historical forecast project: Do stratosphere-resolving models make better seasonal climate predictions in boreal winter? *Quarterly Journal of the Royal Meteorological Society*, *142*(696), 1413–1427.

Butler, A. H., & Gerber, E. P. (2018). Optimizing the definition of a sudden stratospheric warming. *Journal of Climate*, *31*(6), 2337–2344.

Butler, A. H., & Polvani, L. M. (2011). El Niño, La Niña, and stratospheric sudden warmings: A reevaluation in light of the observational record. *Geophysical Research Letters*, *38*, L13807. https://doi.org/10.1029/2011GL048084

Butler, A. H., Polvani, L. M., & Deser, C. (2014). Separating the stratospheric and tropospheric pathways of El Niño–Southern Oscillation teleconnections. *Environmental Research Letters*, *9*(2), 024014.

Calvo, N., Giorgetta, M. A., Garcia-Herrera, R., & Manzini, E. (2009). Nonlinearity of the combined warm ENSO and QBO effects on the northern hemisphere polar vortex in MAECHAM5 simulations. *Journal of Geophysical Research*, *114*, D13109. https://doi.org/10.1029/2008JD011445

Calvo, N., Iza, M., Hurwitz, M. M., Manzini, E., Pea-Ortiz, C., Butler, A. H., et al. (2017). Northern hemisphere stratospheric pathway of different El Niño flavors in stratosphere-resolving CMIP5 models. *Journal of Climate*, *30*(12), 4351–4371. https://doi.org/10.1175/JCLI-D-16-0132.1

Cámara, A. d. l., Albers, J. R., Birner, T., Garcia, R. R., Hitchcock, P., Kinnison, D. E., & Smith, A. K. (2017). Sensitivity of sudden stratospheric warmings to previous stratospheric conditions. *Journal of the Atmospheric Sciences*, *74*(9), 2857–2877.

Camp, C. D., & Tung, K. K. (2007). Stratospheric polar warming by ENSO in winter, a statistical study. *Geophysical Research Letters*, *34*, L04809. https://doi.org/10.1029/2006GL028521

Charlton, A. J., & Polvani, L. M. (2007). A new look at stratospheric sudden warmings. Part I: Climatology and modeling benchmarks. *Journal of Climate*, *20*, 449–471. https://doi.org/10.1175/JCLI3996.1

Cheung, H. N., Zhou, W., Mok, H. Y., & Wu, M. C. (2012). Relationship between Ural-Siberian blocking and the East Asian winter monsoon in relation to the Arctic oscillation and the El Niño Southern Oscillation. *Journal of Climate*, *25*(12), 4242–4257. https://doi.org/10.1175/JCLI-D-11-00225.1

Cohen, J., & Jones, J. (2011). Tropospheric precursors and stratospheric warmings. *Journal of Climate*, *24*, 6562–6572. https://doi.org/10.1175/2011JCLI4160.1

De Hoon, M., Van der Hagen, T., Schoonewelle, H., & Van Dam, H. (1996). Why Yule-Walker should not be used for autoregressive modelling. *Annals of nuclear energy*, *23*(15), 1219–1228.
Domeisen, D. I., Butler, A. H., Fröhlich, K., Bittner, M., Müller, W. A., & Baehr, J. (2015). Seasonal predictability over europe arising from El Niño and stratospheric variability in the MPI-ESM seasonal prediction system. *Journal of Climate*, *28*(1), 256–271.
Domeisen, D. I., Garfinkel, C. I., & Butler, A. H. (2019). The teleconnection of El Niño Southern Oscillation to the stratosphere. *Reviews of Geophysics*, *0*(0). https://doi.org/10.1029/2018RG000596
Dunn-Sigouin, E., & Son, S.-W. (2013). Northern Hemisphere blocking frequency and duration in the CMIP5 models. *Journal of Geophysical Research: Atmospheres*, *118*, 1179–1188. https://doi.org/10.1002/jgrd.50143
Free, M., & Seidel, D. J. (2009). Observed El Niño-Southern Oscillation temperature signal in the stratosphere. *Journal of Geophysical Research*, *114*, D23108. https://doi.org/10.1029/2009JD012420
Garfinkel, C. I., Benedict, J. J., & Maloney, E. D. (2014). Impact of the MJO on the boreal winter extratropical circulation vortex. *Geophysical Research Letters*, *41*, 6055–6062. https://doi.org/10.1029/2014GL061094
Garfinkel, C. I., Butler, A. H., Waugh, D. W., & Hurwitz, M. M. (2012a). Why might SSWs occur with similar frequency in El Niño and La Niña winters? *Journal of Geophysical Research*, *117*, D19106. https://doi.org/10.1029/2012JD017777
Garfinkel, C. I., Feldstein, S. B., Waugh, D. W., Yoo, C., & Lee, S. (2012b). Observed connection between stratospheric sudden warmings and the Madden-Julian Oscillation. *Geophysical Research Letters*, *39*, L18807. https://doi.org/10.1029/2012GL053144
Garfinkel, C. I., & Hartmann, D. L. (2007). Effects of the El-Nino Southern Oscillation and the Quasi-Biennial Oscillation on polar temperatures in the stratosphere. *Journal of Geophysical Research*, *112*, D19112. https://doi.org/10.1029/2007JD008481
Garfinkel, C. I., & Hartmann, D. L. (2008). Different ENSO teleconnections and their effects on the stratospheric polar vortex. *Journal of Geophysical Research*, *113*, D18114. https://doi.org/10.1029/2008JD009920
Garfinkel, C. I., & Hartmann, D. L. (2010). The influence of the quasi-biennial oscillation on the north pacific and El-Niño teleconnections. *Journal of Geophysical Research*, *115*, D20116. https://doi.org/10.1029/2010JD014181
Garfinkel, C. I., Hartmann, D. L., & Sassi, F. (2010). Tropospheric precursors of anomalous Northern Hemisphere stratospheric polar vortices. *Journal of Climate*, *23*, 3282–3299. https://doi.org/10.1175/2010JCLI3010.1
Garfinkel, C., & Schwartz, C. (2017). MJO-related tropical convection anomalies lead to more accurate stratospheric vortex variability in subseasonal forecast models. *Geophysical research letters*, *44*, 10,054–10,062. https://doi.org/10.1002/2017GL074470
Garfinkel, C. I., Schwartz, C., Domeisen, D. I., Son, S.-W., Butler, A. H., & White, I. P. (2018). Extratropical atmospheric predictability from the quasi-biennial oscillation in subseasonal forecast models. *Journal of Geophysical Research: Atmospheres*, *123*, 7855–7866. https://doi.org/10.1029/2018JD028724
Gershunov, A., & Barnett, T. P. (1998). Interdecadal modulation of ENSO teleconnections. *Bulletin of the American Meteorological Society*, *79*, 2715–2725.
Gollan, G., & Greatbatch, R. J. (2017). The relationship between Northern Hemisphere winter blocking and tropical modes of variability. *Journal of Climate*, *30*(22), 9321–9337.
Greatbatch, R. J., Lu, J., & Peterson, K. A. (2004). Nonstationary impact of ENSO on Euro-Atlantic winter climate. *Geophysical Research Letters*, *31*, L02208. https://doi.org/10.1029/2003GL018542
Halpert, M. S., & Ropelewski, C. F. (1992). Surface temperature patterns associated with the Southern Oscillation. *Journal of Climate*, *5*, 577–593. https://doi.org/10.1175/1520-0442(1992)005<0577:STPAWT>2.0.CO;2
Hamill, T. M. (2001). Interpretation of rank histograms for verifying ensemble forecasts. *Monthly Weather Review*, *129*(3), 550–560.
Horel, J. D., & Wallace, J. M. (1981). Planetary scale atmospheric phenomena associated with the Southern Oscillation. *Monthly Weather Review*, *109*, 813–829.
Hu, D., & Guan, Z. (2018). Decadal relationship between the stratospheric Arctic vortex and Pacific decadal oscillation. *Journal of Climate*, *31*(9), 3371–3386.
Hu, Z.-Z., Huang, B., Kinter, J. L., Wu, Z., & Kumar, A. (2012). Connection of the stratospheric QBO with global atmospheric general circulation and tropical SST. Part II: Interdecadal variations. *Climate dynamics*, *38*(1-2), 25–43.
Hu, J., Li, T., Xu, H., & Yang, S. (2017). Lessened response of boreal winter stratospheric polar vortex to El Niño in recent decades. *Climate Dynamics*, *49*(1-2), 263–278. https://doi.org/10.1007/s00382-016-3340-z
Huang, B., Thorne, P. W., Banzon, V. F., Boyer, T., Chepurin, G., Lawrimore, J. H., et al. (2017). Extended reconstructed sea surface temperature, version 5 (ERSSTV5): upgrades, validations, and intercomparisons. *Journal of Climate*, *30*(20), 8179–8205.
Hurwitz, M., Newman, P., & Garfinkel, C. (2012). On the influence of North Pacific sea surface temperatures on the Arctic winter climate. *Journal of Geophysical Research*, *117*, D19110. https://doi.org/10.1029/2012JD017819
Ineson, S., & Scaife, A. A. (2009). The role of the stratosphere in the European climate response to El Niño. *Nature-Geo*, *2*, 32–36. https://doi.org/10.1038/ngeo381
Iza, M., Calvo, N., & Manzini, E. (2016). The stratospheric pathway of La Niña. *Journal of Climate*, *29*(24), 8899–8914.
Jiménez-Esteve, B., & Domeisen, D. I. V. (2018). The tropospheric pathway of the ENSO-North Atlantic teleconnection. *Journal of Climate*, *31*(11), 4563–4584. https://doi.org/10.1175/JCLI-D-17-0716.1
Kang, W., & Tziperman, E. (2017). More frequent sudden stratospheric warming events due to enhanced MJO forcing expected in a warmer climate. *Journal of Climate*, *30*, 8727–8743. https://doi.org/10.1175/JCLI-D-17-0044.1
Kren, A., Marsh, D., Smith, A., & Pilewskie, P. (2016). Wintertime Northern Hemisphere response in the stratosphere to the Pacific decadal oscillation using the whole atmosphere community climate model. *Journal of Climate*, *29*(3), 1031–1049.
Kretschmer, M., Runge, J., & Coumou, D. (2017). Early prediction of extreme stratospheric polar vortex states based on causal precursors. *Geophysical Research Letters*, *44*, 8592–8600. https://doi.org/10.1002/2017GL074696
Kumar, A., Jha, B., & L'Heureux, M. (2010). Are tropical SST trends changing the global teleconnection during La Niña? *Geophysical Research Letters*, *37*, L12702. https://doi.org/10.1029/2010GL043394
Li, Y., & Lau, N.-C. (2013). Influences of ENSO on stratospheric variability, and the descent of stratospheric perturbations into the lower troposphere. *Journal of Climate*, *26*(13), 4725–4748. https://doi.org/10.1175/JCLI-D-12-00581.1
Limpasuvan, V., Thompson, D. W. J., & Hartmann, D. L. (2004). The life cycle of the Northern Hemisphere sudden stratospheric warmings. *Journal Climate*, *17*, 2584–2596.
Liu, C., Tian, B., Li, K.-F., Manney, G. L., Livesey, N. J., Yung, Y. L., & Waliser, D. E. (2014). Northern hemisphere mid-winter vortex-displacement and vortex-split stratospheric sudden warmings: Influence of the Madden-Julian Oscillation and quasi-biennial oscillation. *Journal of Geophysical Research: Atmospheres*, *119*, 12,599–12,620. https://doi.org/10.1002/2014JD021876
Manzini, E., Giorgetta, M. A., Kornbluth, L., & Roeckner, E. (2006). The influence of sea surface temperatures on the northern winter stratosphere: Ensemble simulations with the MAECHAM5 model. *Journal Climate*, *19*, 3863–3881.

Masato, G., Hoskins, B. J., & Woollings, T. (2013). Winter and summer Northern Hemisphere blocking in CMIP5 models. *Journal of Climate*, *26*(18), 7044–7059.

Newman, P. A., Nash, E. R., & Rosenfield, J. E. (2001). What controls the temperature of the Arctic stratosphere during the spring. *Journal of Geophysical Research*, *106*, 19,999–20,010.

Omrani, N.-E., Keenlyside, N. S., Bader, J., & Manzini, E. (2014). Stratosphere key for wintertime atmospheric response to warm atlantic decadal conditions. *Climate Dynamics*, *42*(3-4), 649–663. https://doi.org/10.1007/s00382-013-1860-3

Polvani, L. M., & Kushner, P. J. (2002). Tropospheric response to stratospheric perturbations in a relatively simple general circulation model. *Geophysical Research Letters*, *29*(7), 1114. https://doi.org/10.129/2001GL014284

Polvani, L. M., Sun, L., Butler, A. H., Richter, J. H., & Deser, C. (2017). Distinguishing stratospheric sudden warmings from ENSO as key drivers of wintertime climate variability over the North Atlantic and Eurasia. *Journal of Climate*, *30*(6), 1959–1969.

Polvani, L. M., & Waugh, D. W. (2004). Upward wave activity flux as a precursor to extreme stratospheric events and subsequent anomalous surface weather regimes. *Journal of Climate*, *17*, 3548–3554.

Rienecker, M. M., Suarez, M. J., Gelaro, R., Todling, R., Bacmeister, J., Liu, E., et al. (2011). MERRA: NASA's Modern-Era Retrospective Analysis for Research and Applications. *Journal of Climate*, *24*, 3624–3648. https://doi.org/10.1175/JCLI-D-11-00015.1

Ropelewski, C. F., & Halpert, M. S. (1987). Global and regional scale precipitation patterns associated with the El Niño/Southern Oscillation. *Monthly Weather Review*, *115*, 1606. https://doi.org/10.1175/1520-0493(1987)115<1606:GARSPP>2.0.CO;2

Schiemann, R., Demory, M.-E., Shaffrey, L. C., Strachan, J., Vidale, P. L., Mizielinski, M. S., et al. (2017). The resolution sensitivity of Northern Hemisphere blocking in four 25-km atmospheric global circulation models. *Journal of Climate*, *30*(1), 337–358.

Schwartz, C., & Garfinkel, C. I. (2017). Relative roles of the MJO and stratospheric variability in North Atlantic and European winter climate. *Journal of Geophysical Research: Atmospheres*, *122*, 4184–4201. https://doi.org/10.1002/2016JD025829

Shaman, J. (2014). The seasonal effects of ENSO on european precipitation: Observational analysis. *Journal of Climate*, *27*(17), 6423–6438. https://doi.org/10.1175/JCLI-D-14-00008.1

Shaman, J., & Tziperman, E. (2016). The superposition of eastward and westward Rossby waves in response to localized forcing. *Journal of Climate*, *29*(20), 7547–7557. https://doi.org/10.1175/JCLI-D-16-0119.1

Sigmond, M., Scinocca, J., Kharin, V., & Shepherd, T. (2013). Enhanced seasonal forecast skill following stratospheric sudden warmings. *Nature Geoscience*, *6*(2), 98–102. https://doi.org/10.1038/ngeo1698

Sjoberg, J. P., & Birner, T. (2012). Transient tropospheric forcing of sudden stratospheric warmings. *Journal of the Atmospheric Sciences*, *69*(11), 3420–3432. https://doi.org/10.1175/JAS-D-11-0195.1

Smith, K. L., Fletcher, C. G., & Kushner, P. J. (2010). The role of linear interference in the annular mode response to extratropical surface forcing. *Journal Climate*, *23*, 6036–6050. https://doi.org/10.1175/2010JCLI3606.1

Smith, K. L., & Kushner, P. J. (2012). Linear interference and the initiation of extratropical stratosphere-troposphere interactions. *Journal of Geophysical Research*, *117*, D13107. https://doi.org/10.1029/2012JD017587

Song, K., & Son, S.-W. (2018). Revisiting the ENSO–SSW relationship. *Journal of Climate*, *31*(6), 2133–2143.

Taguchi, M., & Hartmann, D. L. (2006). Increased occurrence of stratospheric sudden warming during El Niño as simulated by WAACM. *Journal Climate*, *19*, 324–332. https://doi.org/10.1175/JCLI3655.1

Takaya, K., & Nakamura, H. (2001). A formulation of a phase-independent wave-activity flux for stationary and migratory quasigeostrophic eddies on a zonally varying basic flow. *Journal of the Atmospheric Sciences*, *58*(6), 608–627.

Trenberth, K. E., Branstator, G. W., Karoly, D., Kumar, A., Lau, N.-C., & Ropelewski, C. (1998). Progress during TOGA in understanding and modeling global teleconnections associated with tropical sea surface temperatures. *Journal of Geophysical Research*, *103*, 14,291–14,324.

Vimont, D. J., Battisti, D. S., & Hirst, A. C. (2002). Pacific interannual and interdecadal equatorial variability in a 1000-yr simulation of the csiro coupled general circulation model. *Journal of Climate*, *15*(2), 160–178. https://doi.org/10.1175/1520-0442(2002)015<0160:PIAIEV>2.0.CO;2

Vitart, F., Ardilouze, C., Bonet, A., Brookshaw, A., Chen, M., Codorean, C., et al. (2017). The sub-seasonal to seasonal prediction (S2S) project database. *Bulletin of the American Meteorological Society*, *98*, 1630–173. https://doi.org/10.1175/BAMS-D-16-0017.1

Weinberger, I., Garfinkel, C. I., White, I. P., & Oman, L. (2019). The salience of nonlinearities in the boreal winter response to ENSO: Arctic stratosphere and Europe. *Climate Dynamics*, 1–21. https://doi.org/10.1007/s00382-019-04805-1

White, I., Garfinkel, C. I., Gerber, E. P., Jucker, M., Aquila, V., & Oman, L. D. (2019). The downward influence of sudden stratospheric warmings: Association with tropospheric precursors. *Journal of Climate*, *32*(1), 85–108. https://doi.org/10.1175/JCLI-D-18-0053.1

Woo, S.-H., Sung, M.-K., Son, S.-W., & Kug, J.-S. (2015). Connection between weak stratospheric vortex events and the Pacific decadal oscillation. *Climate dynamics*, *45*(11-12), 3481–3492.

Yang, S., Li, T., Hu, J., & Shen, X. (2017). Decadal variation of the impact of La Niña on the winter Arctic stratosphere. *Advances in Atmospheric Sciences*, *34*(5), 679–684.